IEEE Access
Multidisciplinary | Rapid Review | Open Access Journal

Received September 11, 2017, accepted October 9, 2017, date of publication November 14, 2017, date of current version December 5, 2017.

Digital Object Identifier 10.1109/ACCESS.2017.2773502

Design of Dual-Band Bandpass Filter With High Isolation and Wide Stopband

YA XIE, FU-CHANG CHEN, (Member, IEEE), AND ZHAO LI
School of Electronic and Information Engineering, South China University of Technology, Guangzhou 510640, China

Corresponding author: Fu-Chang Chen (chenfuchang@scut.edu.cn)

This work was supported in part by the National Natural Science Foundation of China under Grant 61571194, in part by the Project of the Pearl River Young Talents of Science and Technology in Guangzhou, in part by the Science and Technology Planning Project of Guangdong Province under Grant 2014A010103013, and in part by the Natural Science Foundation of Guangdong Province under Grant 2015A030313203.

ABSTRACT A simple and effective method to design a dual-band bandpass filter with high isolation and wide stopband is presented and validated using symmetric open-circuited stub-loaded resonators. By adjusting the electric length and the ratio of characteristic admittance of the resonators, the first two resonant frequencies are identical, but the higher order resonant frequencies dispersed in the upper stopband to extent the bandwidth of stopband. Two transmission zeros are introduced to obtain high isolation and selectivity between the two passbands by placing them in the appropriate position. Proper feeding position is selected to further improve the attenuation of stopband. The measured results highly agree with the simulated one. Measured results demonstrate the isolation level of 40 dB, attenuation of larger than 28 dB, and a wide stopband.

INDEX TERMS Dual-band bandpass filter, high isolation, microstrip, stub-loaded resonators, wide stopband.

I. INTRODUCTION

In modern wireless communication systems, microwave filters with dual-band and wide stopband characteristics are desirable to reduce circuit size and cost [1], [2]. Usually, the dual-band bandpass filters can be designed using multi-mode resonators, such as stepped impedance resonators [3], [4] and stub loaded resonators [5]–[7].

To meet the requirement of wide stopband performance, much research regarding the dual-band filters has been carried out. Some are benefit from the different structure of stepped impedance resonator (SIR) and uniform impedance resonator (UIR) like [8]–[10]. Several dual-band filters were designed in [8], in which reveals two controllable passbands and excellent stopband rejection. In [9], the wide stopband is obtained by embedding a lowpass filter at input/output port. However, the rejection level in the upper stopband is not good enough. In [10], a wide stopband dual-band bandpass filter had been developed by selecting the desired impedance and length ratios.

In addition, a popular method is to introduce multiple transmission zeros to achieve the requirement of wide stopband and high rejection level [11]–[14], which is an effective way to meet some particular requirement. Modified coupled line was involved in the dual-band bandpass filter, adding two more transmission zeros to increase the isolation and control the bandwidth of passbands in [11]. Lin *et al.* [12] presented a compact symmetrical dual-band bandpass filter using stub-to-stub coupling, which produce two transmission zeros to obtain wide upper stopband. In [13], based on stub-loaded spiral stepped-impedance resonator, dual-band bandpass filter is presented with multiple transmission zeros to provide high selectivity between passband and extend stopband. In [14], a dual-band bandpass filter was designed with wide stopband by combining E-shaped resonator and T-shaped feedlines to create multi-transmission zeros.

Another main approach is a bit more complicated than the former. In short, the first two resonant frequencies are set as passband frequencies while the higher resonant frequencies are designed to stagger in the upper stopband. Jiang *et al.* [15] turned to design a dual-band filter with identical ratio of f_1/f_o but different f_2/f_o value using the SIRs to realize a wide stopband. A dual-band filter with wide stopband and enhanced rejection level was also proposed using different SIRs, as described in [16].

Combined with the two design methods, a dual-band bandpass filter using symmetric open-circuited stub-loaded

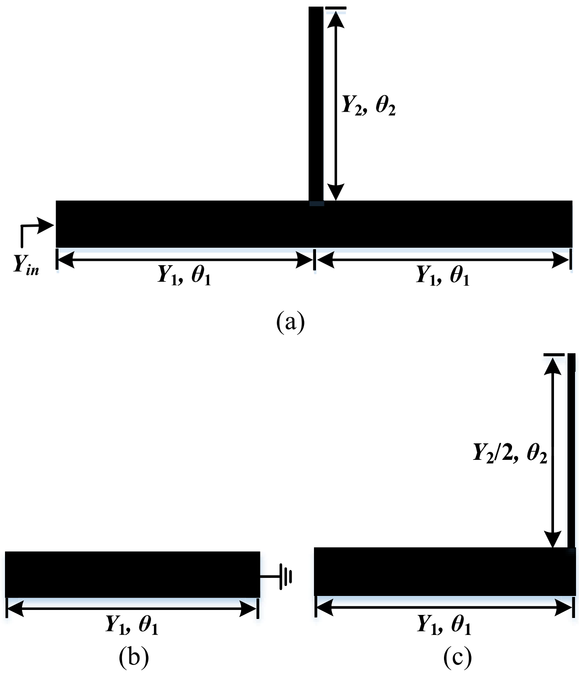

FIGURE 1. (a) Structure of the stub-loaded resonator. (b) Odd-mode equivalent circuit. (c) Even-mode equivalent circuit.

resonators is used to obtain the characteristics of not only high isolation but also wide stopband, and thoroughly analyzed and verified experimentally in this paper.

II. DUAL-BAND FILTER DESIGN

A. RESONANT PROPERTY OF STUB LOADED RESONATOR

The proposed filter comprises of multiple symmetric stub-loaded resonators, and each resonator consists of a half-wavelength transmission line and an open-circuited stub as shown in Fig. 1, where $Y_1, \theta_1, Y_2, \theta_2$ denote the characteristic admittance and electric lengths of the line and open-circuited stub, respectively. The open-circuited stub (Y_2, θ_2) is shunted at the midpoint of the transmission line. Since the open-circuited stub-loaded resonators is symmetrical in structure, odd- and even-mode method can be applied to analyze it. The input admittance of the stub-loaded resonators can be expressed as [5]

$$Y_{\text{in},odd} = -jY_1 \cot\theta_1 \tag{1}$$

$$Y_{\text{in,even}} = \text{j}Y_1 \frac{2Y_1 \tan\theta_1 + Y_2 \tan\theta_2}{2Y_1 - Y_2 \tan\theta_1 \tan\theta_2} \tag{2}$$

From the resonant condition of resonators ($Y_{in,odd} = 0$, $Y_{in,even} = 0$), the stub-loaded resonator is determined by following equations.

$$\cot\theta_1 = 0 \quad \text{(odd-mode)} \tag{3}$$

$$2Y_1\tan\theta_1 + Y_2\tan\theta_2 = 0 \quad \text{(even-mode)} \tag{4}$$

Fig. 2 shows the frequency ratios under different θ_2 and admittance ratio $R_y(Y_1/Y_2)$. By adjusting the electric length and the characteristic admittance, the first two resonant frequencies of R_1 and R_2 are overlapped, and at the same time, the higher order resonant frequencies are staggered in the stopband. This method makes the dual frequencies certain without introducing other structure to suppress unwanted spurious harmonic. From Fig. 2, the realized frequency ration is between 1.06-1.95. To obtain a wider range of f_{even1}/f_{odd1}, stub-loaded stepped impedance resonators can be used [17].

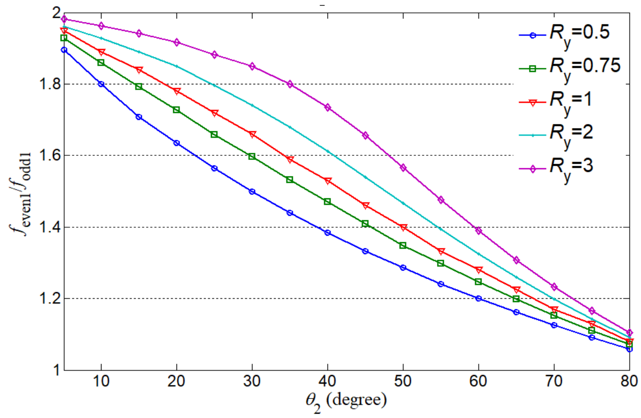

FIGURE 2. Calculated frequency ratios under different open stub lengths and impedance ratios.

Suppose that the first two resonant frequencies of the stub-loaded resonator are f_1 and f_2. According to (3), the odd-mode resonant frequency is only affected by θ_1, and thus, the design procedure should first decide f_1. After that, the second resonant frequency f_2 can be simply controlled by adjusting the length of the open-circuit stub and admittance ratio (Y_1/Y_2) without affecting f_1 according to (4).

According to (3) and (4), the stub-loaded resonators offer independent control of the first two passband f_1 and f_2, thus, the wide stopband dual-band bandpass filter can be realized by staggering the spurious frequencies in the upper stopband.

B. DESIGN OF DUAL-BAND BANDPASS FILTER WITH WIDE STOPBAND

Based on the stub-loaded resonator, a dual-band filter is designed, which is shown in Fig. 3. It consists of two identical stub-loaded resonators (R_1, R_3), placed at left side and the right side, and a different stub-loaded resonator (R_2) in the middle. The coupled feed line used in this design has more degrees of freedom and flexibility in the design process.

The filter in this paper is designed on a conventional substrate of 0.8 mm thickness and with a dielectric constant of 2.55 and a loss tangent of 0.0029. The full wave simulation is carried out by Zeland IE3D.

In this paper, the first two resonant frequencies are set to be 3.5 GHz (f_1), 5.25 GHz (f_2), with third-order Chebyshev response, 0.04321 dB ripple level, 6.5% and 4.3% fractional bandwidth respectively. The element values can be obtained as $g_1 = g_3 = 0.8516$, $g_2 = 1.1032$. So the external quality factors and coupling coefficients can be obtained from the

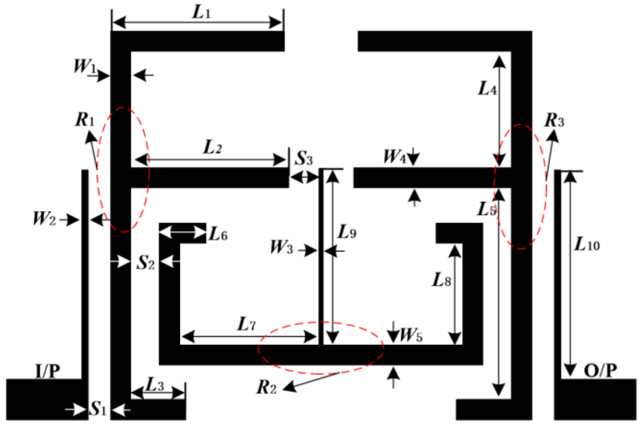

FIGURE 3. Structure of proposed dual-band bandpass filter.

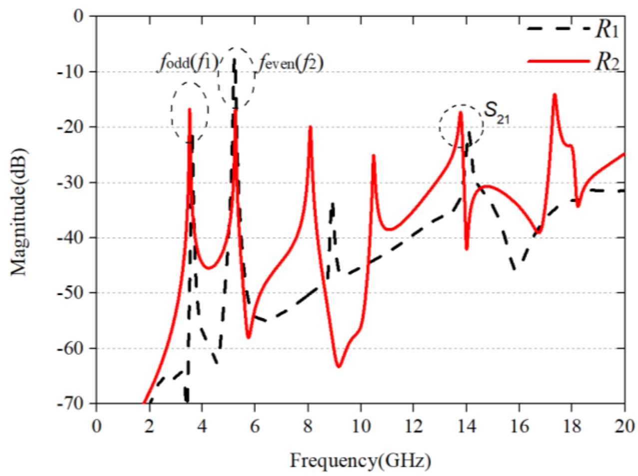

FIGURE 4. Resonant frequencies of different resonators. $W_1 = W_4 = W_5 = 1$ mm, $W_2 = 0.32$ mm.

values of the lowpass prototype. According to the frequency ratio, $R_y = 1$ and $\theta_2 = 42.1°$ can be selected for R_1 while $R_y = 1.9$ and $\theta_2 = 50°$ are selected for R_2. For R_1 and R_3, the characteristic admittances of the half-wavelength transmission line and open-circuited stub are the same ($W_1 = W_4$) while the characteristic admittances of the half-wavelength transmission line and open-circuited stub are different for R_2 ($W_3 \neq W_5$).

The distributions of the resonance frequencies of R_1 and R_2 are plotted in Fig. 4. The first two resonant frequencies of the two resonators are the same (3.5, 5.25 GHz), which are the central frequencies of two passbands. As can be observed, the spurious frequencies of the two different resonators stagger well, which is useful for improving the bandwidth of stopband.

Firstly, we extracted raw data of Q_e using IE3D and the model is shown in the Fig. 5(a). According to the [18, Ch. 7], the external quality factor can be obtained as

$$Q_e = \frac{\omega_0}{\Delta\omega \pm 90°} \tag{5}$$

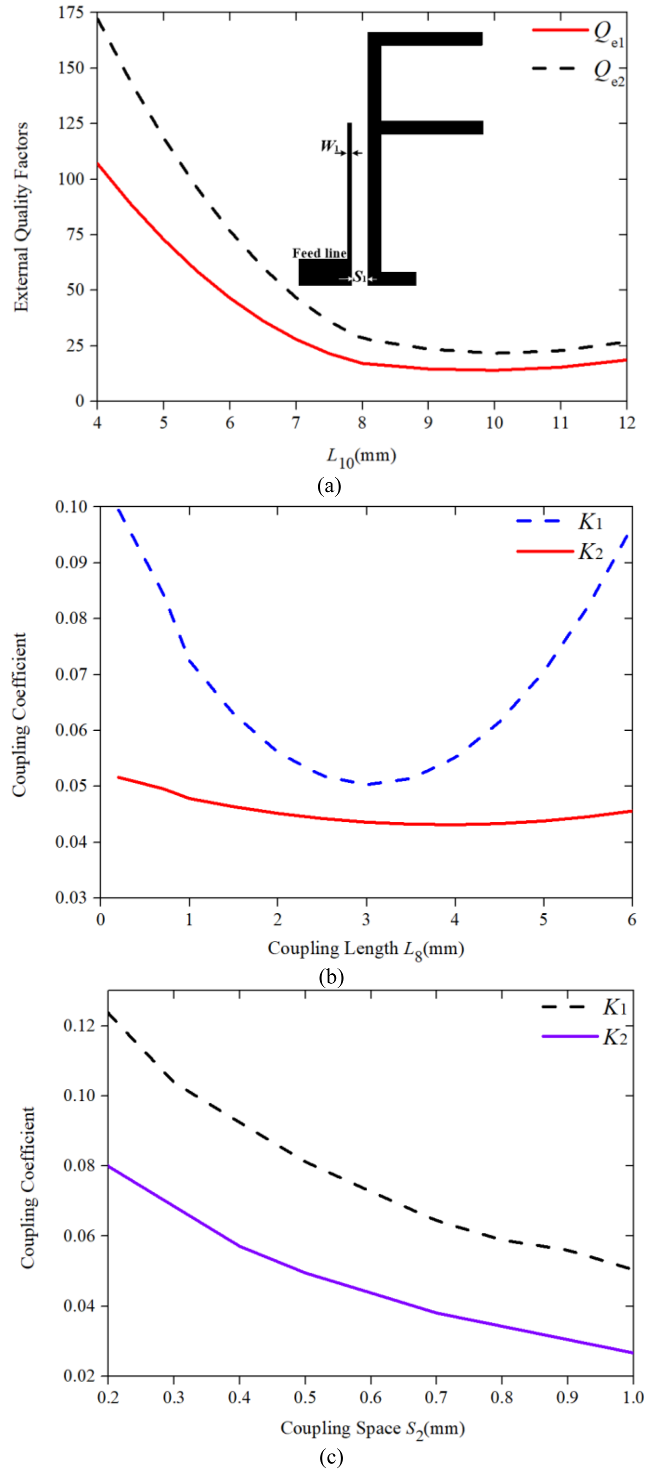

FIGURE 5. Q_e and Coupling coefficients extraction. (a) Q_e. (b) Coupling coefficient under different L_8 ($S_2 = 0.58$ mm). (c) Coupling coefficient under different S_2 ($L_8 = 5$ mm).

Fig. 5 (a) depicts the external quality factor (Q_e) of the two passbands, denoted as Q_{e1} and Q_{e2}. When S_1 and W_2 are fixed ($S_1 = 0.2$, $W_2 = 0.32$), the desired Q_e can be obtained by tuning the coupled-line length (L_{10}). According to the specifications, the required values for the coupling parameter

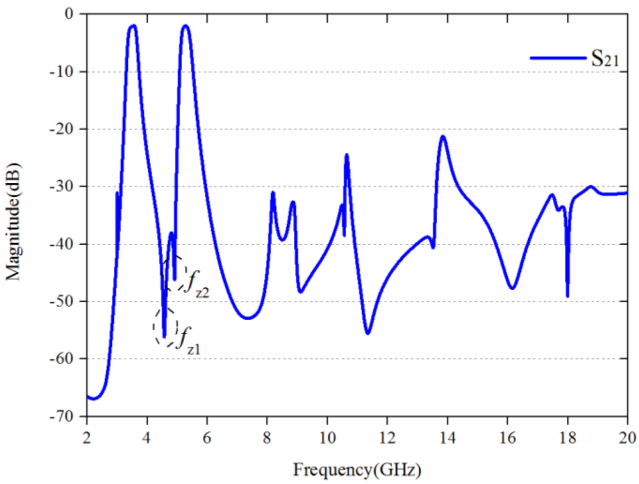

FIGURE 6. **Simulated result with wide stopband. The parameters are as follows (in millimeters): $L_1 = 8.5$, $L_2 = 7.71$, $L_3 = 0$, $L_4 = 5.70$, $L_5 = 14.05$, $L_6 = 2.30$, $L_7 = 6.82$, $L_8 = 4.99$, $L_9 = 8.67$, $L_{10} = 3.68$, $L_{11} = 10.27$, $W_1 = W_4 = W_5 = 1$, $W_2 = 0.32$, $W_3 = 0.2$, $S_1 = 0.2$, $S_2 = 0.58$, $S_3 = 0.71$.**

are $Q_{e1} = 13.1$, $Q_{e2} = 19.8$. Thus, $L_{10} = 10.27$ mm is chosen for the required coupling.

Likewise, the coupling coefficient can be extracted by the formula proposed in [18] from the simulated transmission responses.

$$K = \pm\frac{f_{p2}^2 - f_{p1}^2}{f_{p2}^2 + f_{p1}^2} \tag{6}$$

Extracted coupling coefficients are also plotted in Fig. 5(b) and (c). K_1 and K_2 denote the coupling coefficients at f_1 and f_2, respectively. $K_1 = 0.066$ and $K_2 = 0.044$ can be calculated from the specification. Proper coupling length (L_8) and space (S_2) can be selected according to Fig. 5.

The bandwidth of the filter is determined by the external quality factor and the coupling coefficient between the resonators [17]. According to the analysis above, the overall design procedure are as follows.

Step 1: Determine the length of half-wavelength transmission line, open-circuit stub as well as admittance ratio (Y_1/Y_2) according to required resonant frequencies of two passbands.

Step 2: Select appropriate coupling gap and length (S_2, L_8) to meet the required coupling coefficients of each passband.

Step 3: Select proper combination of L_{10}, W_2, and S_1 to meet the required Q_e of each passband.

Fig. 6 shows the simulated S_{21} of the proposed dual-band filter. A rejection level larger than 20 dB is obtained within the stopband up to 20 GHz. According to Fig. 5, the realizable external quality factors and coupling coefficient are in a wide range. Here, another dual-band filter with wider bandwidths (11.4% and 8.9%) is designed and simulated for demonstration. The comparison of the S-parameters are shown in Fig. 7. The bandwidth of the new filter is expanded while the impedance matching is kept below −20 dB in passband.

Meanwhile, two transmission zeros between the passbands are introduced according to Figs. 6 and 7, which highly

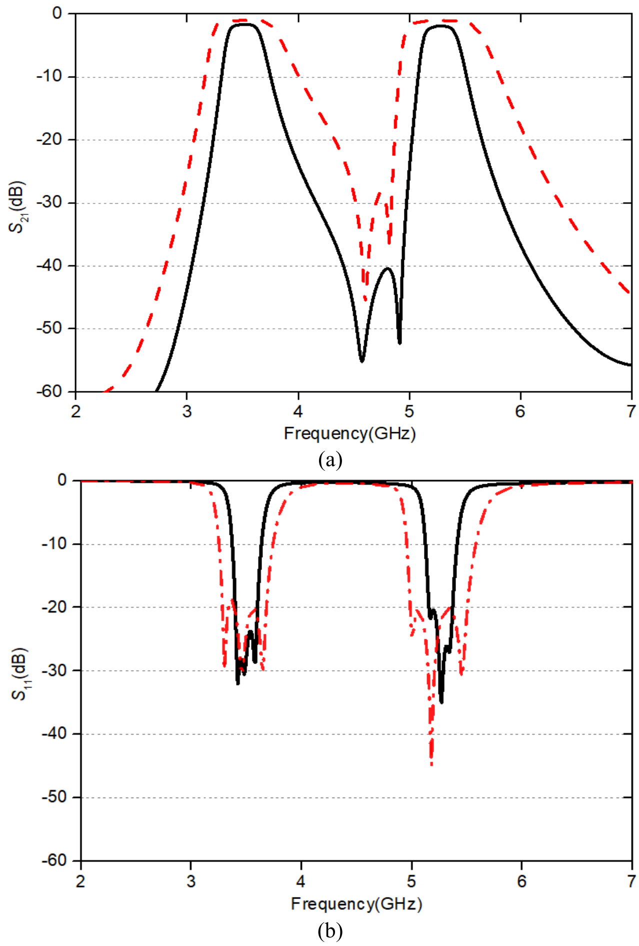

FIGURE 7. **The bandwidth comparison. (a) S_{21}. (b) S_{11}. The parameters of the wider bandwidth filter are as follows (in millimeters): $L_1 = 8.1$, $L_2 = 7.18$, $L_3 = 2.28$, $L_4 = 5.75$, $L_5 = 10.4$, $L_6 = 1.20$, $L_7 = 7$, $L_8 = 5.49$, $L_9 = 8.60$, $L_{10} = 10.67$, $W_1 = W_4 = W_5 = 1$, $W_2 = 0.22$, $W_3 = 0.2$, $S_1 = 0.1$, $S_2 = 0.2$, $S_3 = 0.26$.**

improve the isolation. The first transmission zero (f_{z1}) is produced by the open-circuited stubs [19]. When L_2 is shorter than $\lambda_g/4$ at the first resonant frequency, f_{z1} can be placed at the upper stopband. As shown in Fig. 8, when L_2 varies from 6.0 mm to 7.0 mm, f_{z1} tends to move to the lower frequency. The second zero (f_{z2}) is due to the cross coupling between R_1 and R_3 [20] for the second passband. Path I (R_1-R_2-R_3) is the primary coupling path and path II (R_1-R_3) is the cross coupling route. For the second passband, the coupling between resonators is capacitive. According to [20], the phase shift can be found as

$$\Phi_{21} \approx +90^\circ \quad \text{(resonators below resonance)} \tag{7}$$
$$\Phi_{21} \approx -90^\circ \quad \text{(resonators above resonance)} \tag{8}$$
$$\Phi_{21} \approx +90^\circ \quad \text{(capacitive coupling)} \tag{9}$$
$$\Phi_{21} \approx -90^\circ \quad \text{(inductive coupling)} \tag{10}$$

The total phase shifts are given in Table 1. Below resonance, the two paths are out of phase, but above resonance, the two paths are in phase. It is exactly the destructive

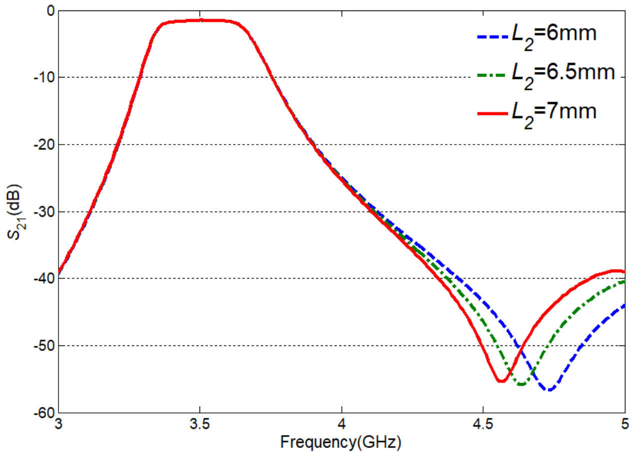

FIGURE 8. The position of the frist transmission zero under different L_2.

TABLE 1. Total phase shifts for two paths of the first passband.

	Below Resonance	Above Resonance
Path 1-2-3	$+90^\circ+90^\circ+90^\circ$	$+90^\circ-90^\circ+90^\circ$
Path 1-3	$+90^\circ$	$+90^\circ$
Result	Out of phase	In phase

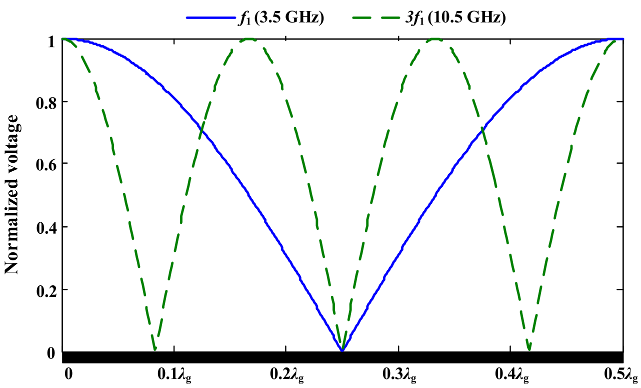

FIGURE 9. Normalized voltage of the half-wavelength resonator at different frequencies.

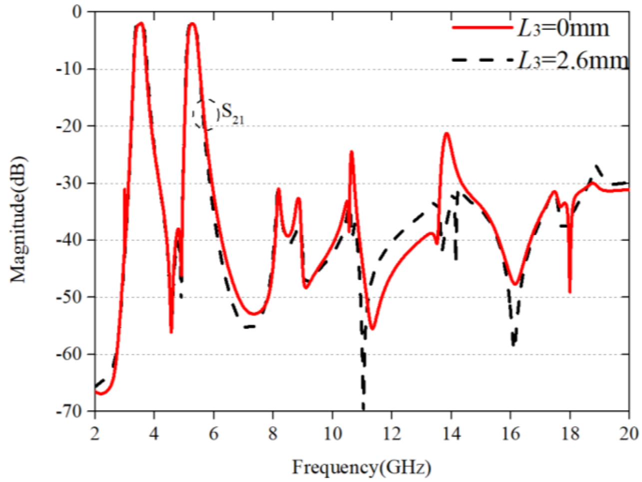

FIGURE 10. Stopband performance of the dual-band filter under different feeding positions.

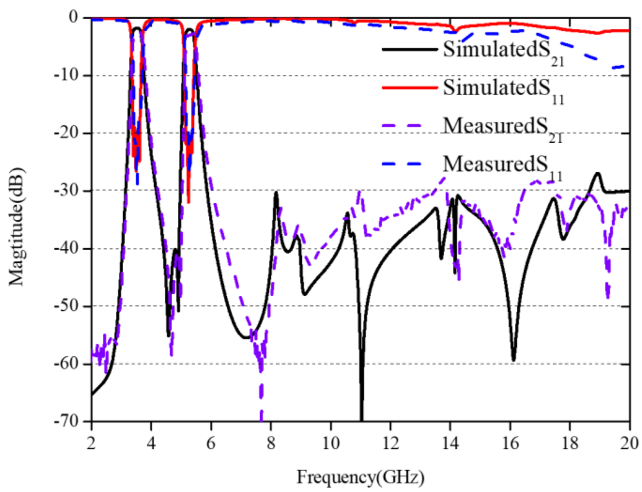

FIGURE 11. Simulated and measured results.

interference that causes a transmission zero on the lower skirt. From the analysis above, it is thus clear that f_{z2} is produced and occurs below the passband.

C. STOPBAND PERFORMANCE ENHANCEMENT

According to Fig. 6, the stopband attenuation is only larger than 20 dB, which is not enough for some applications. To enhance the stopband performance, proper feeding point can be selected to further suppress the harmonics [21]. Fig. 9 shows a half-wavelength resonator with normalized voltage at the first and third resonant frequencies (f_1, $3f_1$), where λ_g is the guided wavelength at f_1. There is voltage zero (λ_g /12) at $3f_1$, so the harmonic at $3f_1$ can be properly suppressed by tuning L_3. Fig. 10 shows the simulated transmission response of the dual-band filter under different feeding positions, which verify the above concept. A bonus rejection improvement is observed at $4f_1$ because of similar mechanism.

III. SIMULATED AND MEASURED RESULTS

Based on the analysis on the above, a dual-band filter with wide stopband is designed and fabricated to verify the application. The center frequencies of the dual-band filter are 3.50 GHz and 5.25 GHz. The fractional bandwidths are 6.5% and 4.3% (0.04321 dB ripple level). The optimized parameters in Fig. 3 are (unit: mm): $L_1 = 8.5$, $L_2 = 7.71$, $L_3 = 2.6$, $L_4 = 5.70$, $L_5 = 10.4$, $L_6 = 2.30$, $L_7 = 6.82$, $L_8 = 5$, $L_9 = 8.67$, $L_{10} = 10.27$, $W_1 = W_4 = W_5 = 1$, $W_2 = 0.32$, $W_3 = 0.2$, $S_1 = 0.2$, $S_2 = 0.58$, $S_3 = 0.71$.

Fig. 11 shows the simulated and measured results while the measurement was carried out on HP 5320A vector network analyzer. The 3 dB fractional bandwidth of two passbands are 3.34 GHz to 3.63 GHz, 5.15 GHz to 5.40 GHz, respectively.

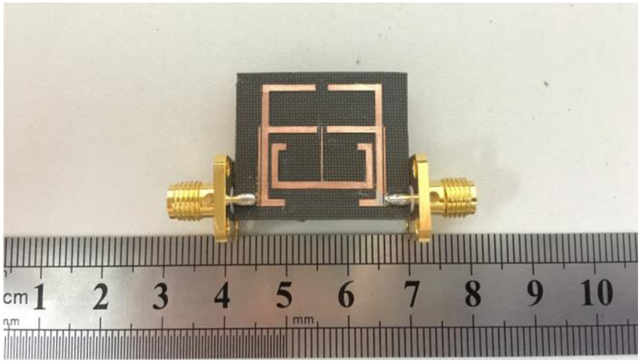

FIGURE 12. Fabricated dual-band filter.

TABLE 2. Performance comparison of the dual-band filter with the state of the art.

Filter	Passbands (GHz)	Upper Stopband	Size (mm^2)	Insertion loss Return loss
9	2.2/5.8	9.7f_1(>20 dB)	30 x 15	0.96/2.6 14.2/13.8
10	1.39/1.82	5.6 f_1 (>20 dB)	60 x 60	2.48/3.6 >20
12	1.5/2.4	3.9 f_1 (>20 dB)	27 x 20	1.1/0.9 >20
13	0.35/0.90	6.5 f_1 (>19 dB)	31 x 21	1.6/1.4 14/17
This work	3.5/5.25	5.7 f_1 (>28 dB)	27 x 19	1.87/2.33 >20

The insert loss of the first passband is 1.87 dB but 2.33 dB for the second passband and the return loss are both greater than 20 dB. The dual-band filter provides a high attenuation of 28 dB up to 5.7 times the first passband frequency. Furthermore, two transmission zeros can be observed between two passbands. Thus, high isolation (>40 dB) is obtained. Fig. 12 shows the photograph of the fabricated filter. The total size is 27.0 mm × 19 mm, which is approximately $0.459\lambda g \times 0.323\lambda g$, where λg is the guided wavelength on the substrate at f_1. Compared with previous works, the merits of the dual-band filter are its rejection level, wide stopband, and compact size, as shown in table 2.

IV. CONCLUSION

This paper proposes a straightforward method to design a dual-band filter with high isolation and wide stopband. By properly adjusting the electric length and the admittance ratio of the half-wavelength transmission line and the open-circuited stub, the higher order spurious frequencies stagger in the upper stopband, resulting in the wide stopband. Furthermore, through exploring the effect of feeding position and cross coupling, the stopband performance is further improved. The measured results show that the isolation between passbands is greater than 40 dB and the attenuation of multiple harmonics can achieve to approximately 28 dB.

REFERENCES

[1] S.-F. R. Chang *et al.*, "A dual-band RF transceiver for multistandard WLAN applications," *IEEE Trans. Microw. Theory Techn.*, vol. 53, no. 3, pp. 1048–1055, Mar. 2005.

[2] S.-J. Sun, T. Su, B. Wu, and C.-H. Liang, "Compact microstrip dual-band bandpass filter using a novel stub-loaded quad-mode resonator," *IEEE Microw. Wireless Compon. Lett.*, vol. 23, no. 9, pp. 465–467, Sep. 2013.

[3] J.-T. Kuo, T.-H. Yeh, and C.-C. Yeh, "Design of microstrip bandpass filters with a dual-passband response," *IEEE Trans. Microw. Theory Techn.*, vol. 53, no. 4, pp. 1331–1337, Apr. 2005.

[4] S. Sun and L. Zhu, "Compact dual-band microstrip bandpass filter without external feeds," *IEEE Microw. Wireless Compon. Lett.*, vol. 15, no. 10, pp. 644–646, Oct. 2005.

[5] X. Y. Zhang, J.-X. Chen, Q. Xue, and S.-M. Li, "Dual-band bandpass filters using stub-loaded resonators," *IEEE Microw. Wireless Compon. Lett.*, vol. 17, no. 8, pp. 442–444, Jul. 2007.

[6] P. Mondal and M. K. Mandal, "Design of dual-band bandpass filters using stub-loaded open-loop resonators," *IEEE Trans. Microw. Theory Techn.*, vol. 56, no. 1, pp. 150–155, Jan. 2008.

[7] H. W. Liu, S. Li, and B. P. Ren, "Microstrip dual-band bandpass filter with E-shaped multimode resonator," *Electron. Lett.*, vol. 49, no. 14, pp. 887–888, Jul. 2013.

[8] M. Mokhtaari, K. Rambabu, J. Bornemann, and S. Amari, "Advanced stepped-impedance dual-band filters with wide second stopbands," in *Proc. Asia–Pacific Microw. Conf.*, 2007, pp. 2285–2288.

[9] C. W. Tang, H. X. Lu, and C. T. Tseng, "Design of a dual-band bandpass filter with a wide stopband," *Electron. Lett.*, vol. 49, no. 10, pp. 661–662, May 2013.

[10] J. Shi, L. L. Lin, J.-X. Chen, H. Chu, and X. Wu, "Dual-band bandpass filter with wide stopband using one stepped-impedance ring resonator with shorted stubs," *IEEE Microw. Wireless Compon. Lett.*, vol. 24, no. 7, pp. 442–444, Jul. 2014.

[11] C.-W. Tang, C.-T. Tseng, S.-H. Chiu, and P.-H. Wu, "Design of wide passband/stopband microstrip bandpass filters with the stepped coupled line," *IEEE Trans. Microw. Theory Techn.*, vol. 61, no. 3, pp. 1095–1103, Mar. 2013.

[12] L. Lin, S.-J. Sun, B. Wu, and C.-H. Liang, "Dual-band bandpass filter with wide upper stopband using quad-mode stepped impedance stub-loaded resonator," *Electron. Lett.*, vol. 50, no. 16, pp. 1145–1146, Jul. 2014.

[13] V. Singh, V. K. Killamsetty, and B. Mukherjee, "Compact dual-band BPF with wide stopband using stub-loaded spiral stepped-impedance resonator," *Electron. Lett.*, vol. 52, no. 22, pp. 1860–1862, Oct. 2016.

[14] J. Wang, L. Ge, K. Wang, and W. Wu, "Compact microstrip dual-mode dual-band bandpass filter with wide stopband," *Electron. Lett.*, vol. 47, no. 4, pp. 263–265, Feb. 2011.

[15] M. Jiang, H.-P. Lin, and J.-T. Kuo, "Design of quasi-elliptic function filters with dual-passband responses and multi-spurious suppression," in *Proc. Asia–Pacific Microw. Conf.*, pp. 2365–2368, 2007.

[16] J. T. Kuo and H. P. Lin, "Dual-band bandpass filter with improved performance in extended upper rejection band," *IEEE Trans. Microw. Theory Techn.*, vol. 57, no. 4, pp. 824–829, Apr. 2009.

[17] F. C. Chen and Q. X. Chu, "Novel multistub loaded resonator and its application to high-order dual-band filters," *IEEE Trans. Microw. Theory Techn.*, vol. 58, no. 6, pp. 1551–1556, Jun. 2010.

[18] J.-S. Hong and M. J. Lancaster, *Microstrip Filter for RF/Microwave Applications*. New York, NY, USA: Wiley, 2001.

[19] L. Zhu and W. Menzel, "Compact microstrip bandpass filter with two transmission zeros using a stub-tapped half-wavelength line resonator," *IEEE Microw. Wireless Compon. Lett.*, vol. 13, no. 1, pp. 16–18, Jan. 2003.

[20] J. B. Thomas, "Cross-coupling in coaxial cavity filters—A tutorial overview," *IEEE Trans. Microw. Theory Techn.*, vol. 51, no. 4, pp. 604–611, Apr. 2003.

[21] F.-C. Chen, H.-T. Hu, J.-M. Qiu, and Q.-X. Chu, "Cascaded triplet filter using mixed electric and magnetic coupling structure with wide stopband performance," *Microw. Opt. Technol. Lett.*, vol. 56, no. 12, pp. 2937–2940, Dec. 2014.

YA XIE was born in Heyuan, China, in 1994. She is currently pursuing the B.S. degree at the South China University of Technology, Guangzhou, China. Her research interests include microwave filters and associated RF circuits for microwave and millimeter-wave applications.

FU-CHANG CHEN (M'12) was born in Fuzhou, China, in 1982. He received the Ph.D. degree from the South China University of Technology, Guangzhou, China, in 2010. He is currently an Associate Professor with the School of Electronic and Information Engineering, South China University of Technology. His research interests include the synthesis theory and design of microwave filters and associated RF modules for microwave and millimeter-wave applications.

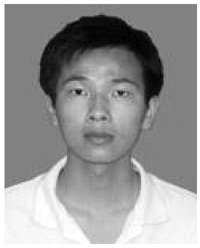

ZHAO LI received the B.S. degree in information engineering from the Wuhan University of Technology, Wuhan, China, in 2016. He is currently pursuing the M.E. degree at the South China University of Technology, Guangzhou, China. His research interests include microwave filters and associated RF circuits for microwave and millimeter-wave applications.